Polarization ratio and effective mass in InP nanowires: Effect of crystallographic axis

Dileep Karanth and Huaxiang Fu
Department of Physics, University of Arkansas, Fayetteville, Arkansas 72701, USA
(Received 20 March 2006; revised manuscript received 29 August 2006; published 16 October 2006)

Indium phosphide nanowires grown along different crystallographic axes—namely, the [001], [101], and [111] directions of zinc-blende structure—are investigated using a first-principles derived semi-empirical pseudopotential theory, aimed at understanding the effects of wire orientation on band structure, polarization ratio, and effective masses of semiconductor nanowires. Band energies over entire Brillouin zone are determined, and are found to exhibit different characteristics for three types of wires in terms of band dispersion and the location of orbital energy. A pronounced dispersion hump is revealed to exist in the lowest conduction band for the [001] and [111] wires, but not for the [101] wires. On the other hand, the [001] and [111] wires are shown to have very different orbital energy for the top valence state at the zone boundary *X* point—being −6.8 eV in the former and −6.2 eV in the latter. These differences provide specific and useful suggestion to encourage experimental determination of the band structure in InP nanowires. As another key result, we study the polarization ratio in wires of different orientations. Our calculations show that, given the same lateral size, the [111] wires yield the highest polarization ratio as compared to wires along the other two directions, while simultaneously possessing larger band-edge photoluminescence transition intensity. The [111] wires are thus suggested to be better suitable for optical device applications. Interestingly, we also found that polarization ratio displays a different size dependence than transition intensity does. More specifically, the polarization ratio is predicted to increase with the decreasing size, which is opposite to the behavior as exhibited by the optical transition intensity. The polarization ratios in the [101] and [111] wires of 11.7 Å diameter are shown to approach the limit of 100%. In addition to polarization ratio, we further determine the electron and hole masses for wires of different crystallographic axes. For the [101] and [111] wires, the hole masses are revealed to be ~0.25, which are markedly smaller than the values (≥1.0) along the same direction in bulk. This result demonstrates an interesting possibility of obtaining in nanowires a high hole mobility that is not available in bulk. An explanation for the anomaly in the hole mass is suggested and is associated with the existence of an electronic band transition.

DOI: 10.1103/PhysRevB.74.155312 PACS number(s): 73.22.−f, 78.67.−n, 73.21.Hb

I. INTRODUCTIONS

Semiconductor wires with lateral size on the nanometer scale are of obvious importance for the eventual development of logic nanocircuits[1–4] and semiconductor nanowire lasers,[5,6] as well as for the generation of photo induced current in photodetector devices,[7] which explains the need of understanding their electronic and optical properties. With respect to three dimensionally confined nanoparticles, nanowires (NW) are better suitable for the purpose of these applications, since (1) the existence of a large conductivity upon doping along the longitudinal wire axis allows carriers easy to transmit, and meanwhile, (2) quantum confinement along the lateral directions offers property tunability as well as efficiency enhancement. Nevertheless, theoretical studies and understanding on nanowires are much less than those on nanodots.[8–19]

One additional and possibly interesting degree of freedom—which exists in wires but not prominently in nanoparticles, and may potentially be useful in modifying the properties of wires—is the crystallographic orientation of the wire axis. Different wires, with an equal diameter and yet formed along different axes (for instance, along the [111] or [101] directions of the zinc-blende structure), may show distinctive traits on band-edge wave function symmetry, luminescence wavelength, and/or transition intensity. It may thus be likely that only some wires along a certain orientation, but not others, can lead to preferable properties.

Another special property in NWs concerns the polarization ratio associated with optical absorption or emission. Different from photoluminescence (or absorption) intensity, polarization ratio often offers considerably higher resolution contrast and sensitivity,[20,21] thereby being a more preferable quantity for use in sensors and optical communication. Recently, highly polarized luminescence, with a giant polarization ratio as high as ~95%, was reported in single InP free-standing nanowires.[7] The observed strong polarity was explained in terms of dielectric confinement, in which a smaller dielectric susceptibility of the environment surrounding nanowires allows the electric field of excitation laser to penetrate effectively into the wires only when the field is polarized along the wire axis.

Here it is useful to point out that the dielectric confinement model depends little on the explicit electronic structure of wires, and is more an extrinsic mechanism than an intrinsic one. Another mechanism that is able to cause a strong polarization of absorption involves the intrinsic electronic states of each individual wire. More specifically, when the dipole matrix elements between band-edge states show significant dependence on the polarization direction of the excitation electric field, the polarity of absorption occurs. This mechanism was originally proposed and demonstrated in Refs. 13–15 for embedded semiconductor quantum wires as a result of confinement induced heavy-hole–light-hole mixing, and was later examined in Refs. 16–18 for free-standing wires. The second mechanism could reveal more insight in

terms of understanding the microscopic electronic properties in semiconductor nanowires. In previous studies of polarization ratio for free-standing nanowires,[17,18] only the [111] wires were investigated using tight-binding or $k \cdot p$ theory. Our concern here centers on how a change in the crystallographic axis of wire may affect the optical polarization ratio. The answer to this question may tell us whether it is possible to improve the polarization ratio by engineering the orientation of nanowire. Since the energy separation between heavy hole and light hole (thus their coupling) depends on the wire orientation, the polarization ratio in wires of different crystallographic axes may thus vary.

A third special property of semiconductor nanowires is electron and/or hole effective mass, which determines carrier mobility and performance speed of nanowire devices. As a question of particular relevance, one may like to know whether it is possible to obtain in nanowires an (electron or hole) effective mass that is considerably *smaller* than in bulk, assuming that carrier moves along the same crystallographic direction in both systems. If this turns out to be feasible, it may lead to faster nanodevice performance that is not available in bulk. Previous studies show that this is indeed possible in strained quantum *wells*, because heavy hole and light hole couple differently with strain.[22,23] However, there is no strain in free-standing nanowires, and further, electronic structure in wires is generally different from in quantum wells. This explains why obtaining a small effective mass in nanowires is particularly interesting. Another question relevant to our present study is the relative carrier mass in nanowires of different crystallographic axes. For most III-V bulk materials, the effective mass of hole is known to be much smaller along the [001] direction than along the [101] or [111] directions.[24] Does this trend and knowledge apply to nanowires? In other words, can we reasonably assume that the [001] wires remain to have a much smaller mass and are thus better suitable for achieving fast device performance than the wires along two other directions? Finally, to gain a better understanding of effective mass in nanowires, one may also wonder whether it is possible to seek a general rule that governs the magnitude of effective mass in these nanostructures. This rule, if available, may be of some value in assisting the analysis and design of carrier mobility in semiconductor nanowires.

In this paper we intend to address the above questions that could be useful towards a better and more comprehensive understanding of semiconductor nanowires, by performing pseudopotential studies of InP wires grown along different crystallographic axes and of different sizes. Our results show that varying crystallographic axis indeed is able to introduce considerable difference to optical transition intensity, polarization ratio, and carrier effective mass in nanowires, thereby offering another possible route to engineer their properties in addition to varying size and/or dimensionality. More specifically, we find that the [111] wires, as compared to wires along other directions, are capable of yielding both stronger band-edge optical intensity and higher polarization ratio as the size of wire becomes smaller. Our study further reveals that, for a given mobility direction, effective mass in nanowires can be markedly smaller than in bulks, which provides a feasibility and useful theoretical support to encourage experimental design of seeking faster performance in nanowire circuits. Though reduced mass is possible both in strained quantum wells[22,23] and in free-standing nanowires, we found that they result from different origins. Moreover, we demonstrate that the observed strong polarity in InP nanowires can be explained by intrinsic electronic properties. Polarization ratio in nanowires is further shown to depend on wire diameter in an opposite fashion as compared to transition intensity. Some of our results turn out to be rather unexpected, for instance, the relative trend of effective mass in *bulks* cannot be straightforwardly applied to the nanowires. We hope that the current study can add some useful knowledge on semiconductor nanowires, in addition to those existing in literature.

II. THEORETICAL METHODS

To describe the band structure of semiconductor wires, one would ideally prefer a direct first-principles density functional theory (DFT),[25] which allows one to take into account the charge redistribution occurring both inside and at the surfaces of nanostructures. One may further prefer to perform quasiparticle calculations[26] so that the theoretical results of optical excitation can be directly compared with experimental measurements. On the other hand, the computation of direct first-principles approaches is generally very time consuming, which limits the application only to dots or wires of small size.[8,9,11,27] Furthermore, for some materials such as InAs or InSb, spin-orbit coupling needs to be considered.

Alternative approaches take advantage of the fact that a majority of experiments have been performed on nanostructures that are passivated by organic capping materials. (Also, these passivated nanoparticles or wires are technologically more useful by possessing properties of better quality.) The passivation electrostatically and/or chemically saturates the dangling bonds at the surface, and removes the defect states away from the fundamental band edge via forming bonding and antibonding states. In fully passivated dots or wires, many measured properties are thus mainly "bulklike" in the sense that they originate from the spatial interior of the structures and subject little to surface conditions. These bulklike properties are attracting predominant attention since they are intrinsic and can be effectively controlled by varying size. Surface effects in semiconductor nanostructures, while interesting, vary from sample to sample, however.

For fully passivated semiconductor nanostructures, alternative approaches to determine their electronic structure include charge patching method,[10] LCAO tight-binding,[28–30] pseudopotentials,[31,32] or multiband $k \cdot p$ theory.[12,16,33] Here we determine the band structure and related properties of nanowires using first-principles derived nonlocal screened atomic pseudopotentials (SAP).[34] Unlike bare atomic pseudopotentials,[35] SAP takes into account the charge self-consistency due to formation of chemical bonds (i.e., the screening effects) in solids, and are derived and parameterized from direct first-principles density functional calculations on *bulk* semiconductors of different crystal structures and different cell volumes (thus being transferable).[34] Obvi-

ously, these pseudopotentials thus derived inherit the problem of first-principles local density-functional approximation (LDA) and underestimate the excitation gap. To correct the LDA band gap, these atomic pseudopotentials are then adjusted to reproduce the experimental or quasiparticle excitation gap; it was demonstrated that a small variation of the screened atomic potential near the nuclear core is sufficient to make the gap correction, while keeping wave functions nearly unchanged.[34] In addition to corrected band gap, the SAPs also generate reliable electron and hole effective masses that are close to experimental values. Compared to tight-binding method or empirical pseudopotential, screened pseudopotentials were shown to be able to reproduce accurately the DFT single-particle wave functions,[34] thus better suitable for determining transition matrix and optical properties. Compared to $k\cdot p$ theory which is valid near the zone center, the SAP method yields accurate bulk band dispersion over the entire Brillouin zone. The details of deriving SAP for InP as well as demonstration of the accuracy of the potentials were given in Ref. 34.

Electronic structure (including orbital energies and wavefunctions of individual electron states) in quantum wires is determined by directly solving the Schrödinger equation $\left[-\frac{1}{2}\nabla^2+V(\mathbf{r})\right]\Psi_i(\mathbf{r})=E_i\Psi_i(\mathbf{r})$ for systems with thousands of atoms, using a similar folded Hamiltonian technique as described in Ref. 36, but with spin-orbit interaction included in the Hamiltonian in the present study.[37] Wave functions $\Psi_i(\mathbf{r})$ are expanded using plane waves as bases; the potential $V(\mathbf{r})$ is constructed as a superposition of the SAP pseudopotentials of all atoms in the nanostructures. Surfaces of nanowires are passivated by hydrogenlike atoms.[34] Matrix elements of optical transitions are calculated using realistic wave functions obtained from the Schrödinger equation.

III. RESULTS AND DISCUSSIONS

It is practically difficult to study nanowires with all possible axis orientations. Here we consider three types of InP wires with their axes grown respectively along the crystallographic [001], [101], and [111] directions of the zinc-blende structure as an example, hoping that these studies can yield some general conclusions that are also useful for other directions. These three directions are chosen since the growth of wires is more likely to occur along the axis of high symmetry. For each type of wires, we perform calculations for four different lateral sizes, with diameter D equal to 11.7, 23.3, 35.0, and 46.6 Å.

Band structure of different wires. Figures 1–3 depict the calculated band structure for differently oriented wires of different sizes. For the [001] wires (Fig. 1), we notice the following conclusions. (1) Three wires of larger diameter have a direct band gap at Γ, thereby suitable for lasering or other optical applications. However, the smallest $D=11.7$ Å [001] wire is shown to have an indirect band gap, in which the lowest conduction band is rather flat with its minimum located at non-Γ. (2) For InP wires in the size range of 23.3–46.6 Å, the valence bands are rather parabolic over the Brillouin zone, but the conduction bands are found to exhibit a pronounced hump. The hump is predicted to locate at $\mathbf{k}_{\text{hump}}\approx 0.2\frac{2\pi}{a}$, where $a=5.83$ Å is the lattice constant of bulk InP, for the $D=46.6$ Å wire. The cusp point in band dispersion is of interest, since it generates singularity in density of states and can be further used to study interstate coupling due to band crossing. By use of wave function projection, the electron states at the cusp point are found to have a similar character as the lowest two conduction states in bulk InP at the $\mathbf{k}$ point located near the midway between Γ and X. The energy difference between the cusp point at $\mathbf{k}_{\text{hump}}$ and the conduction band minimum (CBM) at Γ is calculated to be 0.7 eV in the $D=46.6$ Å wire. Based on this large energy difference, we suggest that inverse photoemission experiments may be able to detect the location of this hump and its energy. (3) For two largest wires considered ($D=35.0$ and 46.6 Å), the formation of well separated subbands in the *conduction* states near Γ is evident, which could be utilized for the purpose of making infrared detectors. The energy difference between two lowest subbands at Γ is calculated to be 0.28 eV in the $D=46.6$ Å wire. (4) The lowest conduction state at the zone-*boundary* X point ($\mathbf{k}=0.5$ in Fig. 1) is found to show a sizable dependence on the wire diameter, varying from −3.51 eV in the $D=23.3$ Å wire to −3.83 eV in the $D=46.6$ Å wire. In fact, this 0.32 eV confinement shift for the CBM at X turns out to be significant and comparable with that for the CBM at Γ (0.39 eV) in the same size range. While most studies focus on the confinement energy at zone center, size effect on the electronic states at the zone boundary is less documented and understood, however. The large conduction-state confinement energy at X can be explained by the band dispersion of bulk InP. In fact, the bulk dispersion of the lowest conduction band along the X-W direction is steep for InP,[34] which causes the large energy shift of the X-like conduction state in nanowires. (5) In a notable contrast with the conduction state, examination of the highest *valence* energy at X point in Fig. 1 reveals that it is located near −6.8 eV for three large [001] wires, showing significantly less size dependence.

Compared to the [001] wires, the low-energy conduction bands of the [101] wires do not exhibit a hump, showing instead a crossing of two bands that occurs at $\mathbf{k}\approx 0.25\frac{2\pi}{\sqrt{2}a}$ for the $D=46.6$ Å wire (see Fig. 2). We attribute this difference to the band folding effect which is different along the two crystallographic directions. Furthermore, the highest valence band at the zone boundary in the $D=46.6$ Å [101] wire is determined to be at an energy of −6.2 eV, which is appreciably different from the counterpart (−6.8 eV) in the [001] wire of the same size. For the [111] wires (see Fig. 3), a hump in the conduction band dispersion is found to exist, as in the [001] wires. And the hump is located at $\mathbf{k}\approx 0.3\frac{2\pi}{\sqrt{3}a}$ for the $D=46.6$ Å wire. As with the [101] wires, but unlike the [001] wires, the highest valence band at the zone-boundary X point is predicted to have an orbital energy around −6.2 eV for the $D=46.6$ Å [111] wire. The considerable difference in the top valence-band orbital energy at the zone boundary for differently oriented wires, as revealed by our calculations, could be examined and confirmed in experiments by use of photoemission spectroscopy.[24]

Size dependence of band-edge orbital energies. Energies of the valence band maximum (VBM) and conduction band

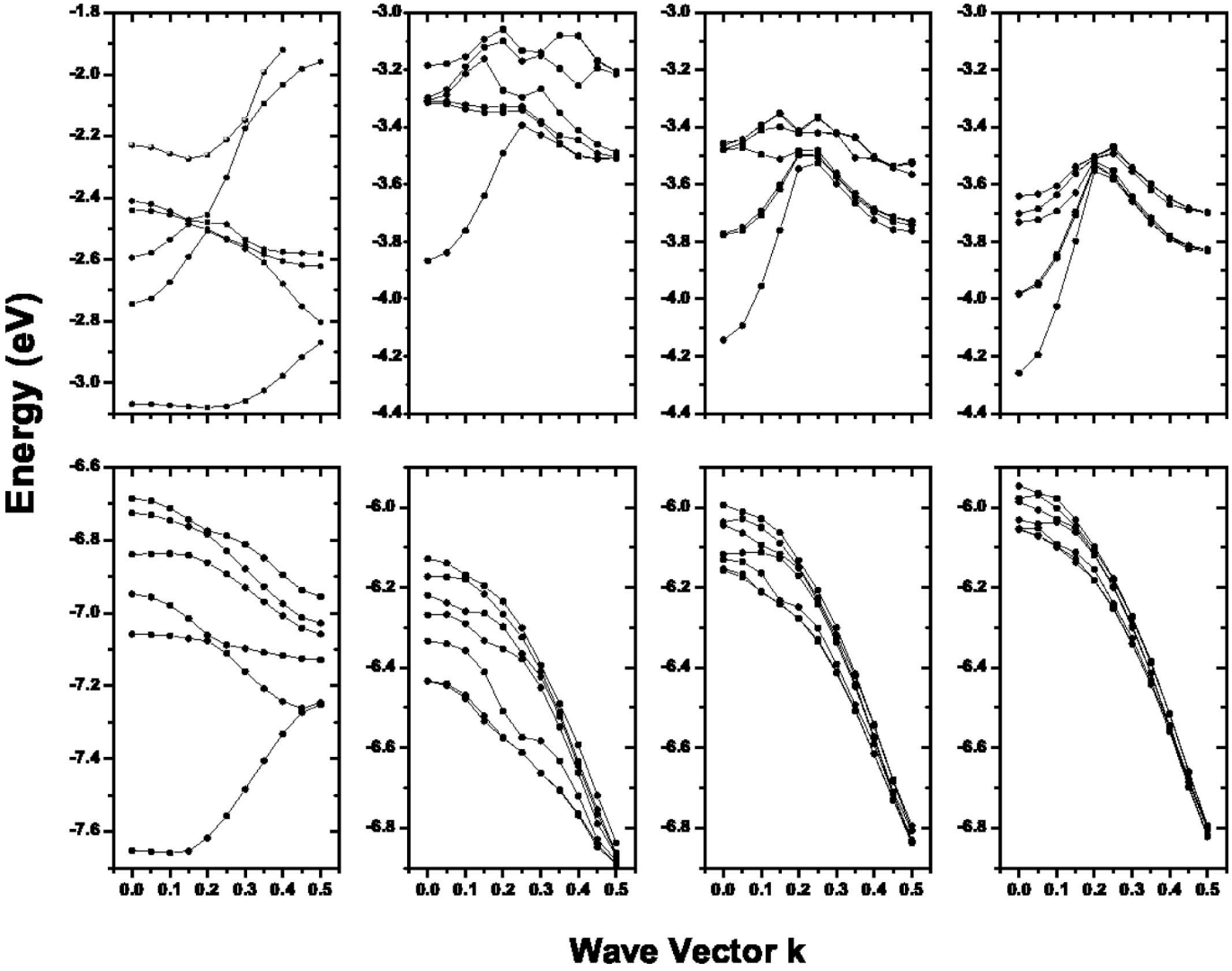

FIG. 1. Band structure of the [001] wires of different sizes. From left to right correspond to the wire of diameter $D=11.7$, 23.3, 35.0, and 46.6 Å, respectively. The zone boundary X point is located at $\mathbf{k}=0.5$. The wave vector is in units of $\frac{2\pi}{a}$, where $a=5.83$ Å is the lattice constant of bulk InP.

minimum (CBM) at Γ are shown in Fig. 4 for each considered wire. To make our calculation results also useful for others, we analytically fit our single-particle energies to $E_i = E_{\text{bulk}} + \frac{A}{D^\alpha}$, and the resulting A and α parameters are given in Table I. We find that the single-particle band gaps obtained in this study generally agree well with the available results from charge patching method[10] and from direct first-principles calculations.[11] For instance, the band-gap shift for the $D=11.7$ Å [111] wire with respect to bulk is determined as 1.69 eV in this study, compared to 1.67 eV in Ref. 10. This value is also close to 1.73 eV from direct DFT calculation for a $D=13.2$ Å [111] wire.[11]

By combining the results in Fig. 4 and in Table I, most notable observations are as follows: (1) The VBM energies of the [101] and [111] wires are very close, not just for small wires but also for large wires (see Fig. 4), though, in bulk InP, the hole effective mass $m_h^*=2.45$ along the [101] direction is considerably larger than the value of $m_h^*=1.03$ along the [111] direction (both masses are calculated from our screened pseudopotentials and agree well with experiments). (2) Interestingly, the α scaling exponents of the VBMs are found to be notably universal ($\alpha \approx 2.7$ with ±5% fluctuation) for wires of *different* crystallographic axes, though the A parameters are different (see Table I). Similarly, the α values ($\alpha \approx 1.2$) of the wire CBMs show also little orientation dependency. (3) To gain a understanding of how the α value depends on dimensionality (instead of the orientation of wire axis), we have also performed calculations for InP spherical *dots* using the same pseudopotentials and passivation, and determine α to be ~1.84 for the VBM and ~0.93 for the CBM. (The A parameter is given in Table I.) This thus demonstrates that the α parameter varies significantly with the dimensionality.

Polarization ratio in nanowires. Let us first examine the transition matrix $T \equiv P_x + P_y + P_z$ at the zone-center Γ point, where $P_i = |\langle \Psi_{\text{VBM}} | \hat{P}_i | \Psi_{\text{CBM}} \rangle|^2$ ($i=x$, y, or z), its dependence on the wire diameter, as well as the effect of crystallographic wire orientation on this quantity. In our study, the z axis is defined to be along the longitudinal axis of the wire. Figure 5 shows the calculated magnitudes of transition matrix ele-

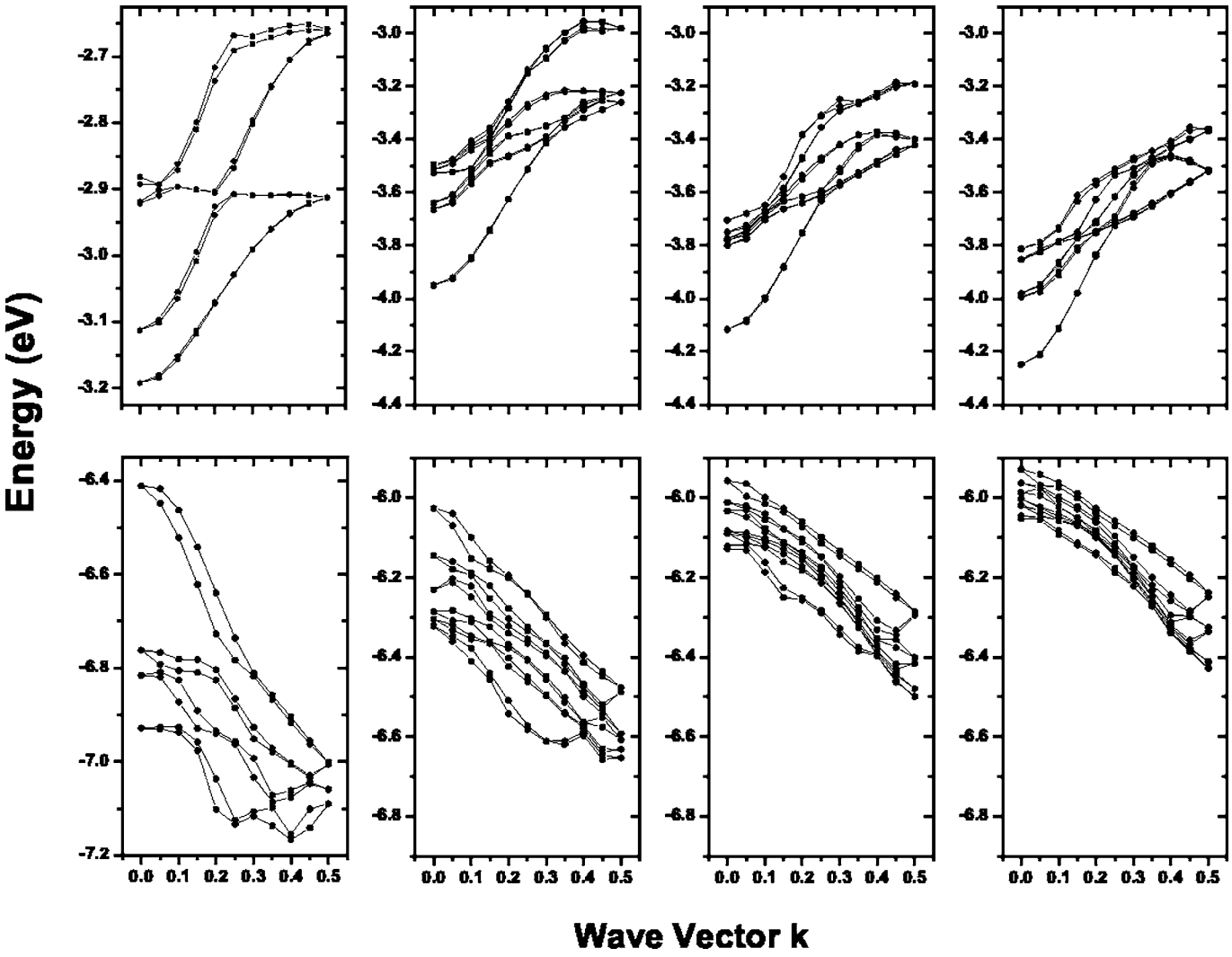

FIG. 2. Same as in Fig. 1, but for the [101] wires of different sizes. The wave vector is in units of $\frac{2\pi}{\sqrt{2}a}$.

ments for differently oriented wires. Notably, one sees that, for each type of wires, the magnitude of the VBM-to-CBM transition matrix T *deceases* as the lateral diameter becomes smaller. This decrease is in difference with the anticipation that the increasing localization of electron and hole wave functions in nanostructures may lead to larger magnitude of transition matrix, as D decreases. Figure 5 further shows that, for wires of large D, the T magnitude does not depend in a significant sense on the orientation of the wire axis. In fact, for the same given diameter $D=46.6$ Å, the T values of the [001], [101], and [111] wires are comparable and all close to 0.5. However, as the size decreases, the T magnitude for the [001] wires is weakened *most* as compared to two other types of wires, by declining to 0.35 in the $D=23.3$ Å [001] wire (the smaller $D=11.7$ Å wire has an indirect band gap). In contrast, the deterioration of the transition magnitude is the least for the [111] wires, and as a result, the $D=23.3$ Å [111] wire remains to have a large T value of 0.45. Our theoretical calculations thus suggest that the [111] wires may be more suitable for maintaining a sharp band-edge absorption (for instance, in the application of photodetection), particularly when smaller size is needed.

Polarization ratio, defined as $P=\frac{P_z-(P_x+P_y)}{P_z+(P_x+P_y)}$, and each component P_i are also shown in Fig. 5, and turn out to be even more interesting. First, for all wires studied (except for the $D=11.7$ Å [001] wire of an indirect band gap), P_x and P_y are notably small, but P_z is not. This gives rise to markedly high polarization ratios in InP nanowires. More specifically, the optical polarization ratio for the $D=11.7$ Å [101] or [111] wire approaches, in a rather remarkable sense, the maximum limit of 100%. Second, and interestingly, for the [101] and [111] wires, the polarization ratio is found to be *enhanced* as the size decreases, in sharp contrast with the total transition magnitude T which changes in an opposite fashion and becomes weaker with the decreasing size. This result thus demonstrates a very distinctive size dependence between polarization ratio and the magnitude of transition matrix in semiconductor quantum wires. The higher polarization ratio in smaller wires also suggests that it is better to utilize this quantity (rather than the intensity) for the purpose of nanowire sensors. The increasing polarization ratio with decreasing size is also true for the [001] wires, except for the indirect $D=11.7$ Å wire. Furthermore, by contrasting the transition magnitude and polarization ratio in wires of differ-

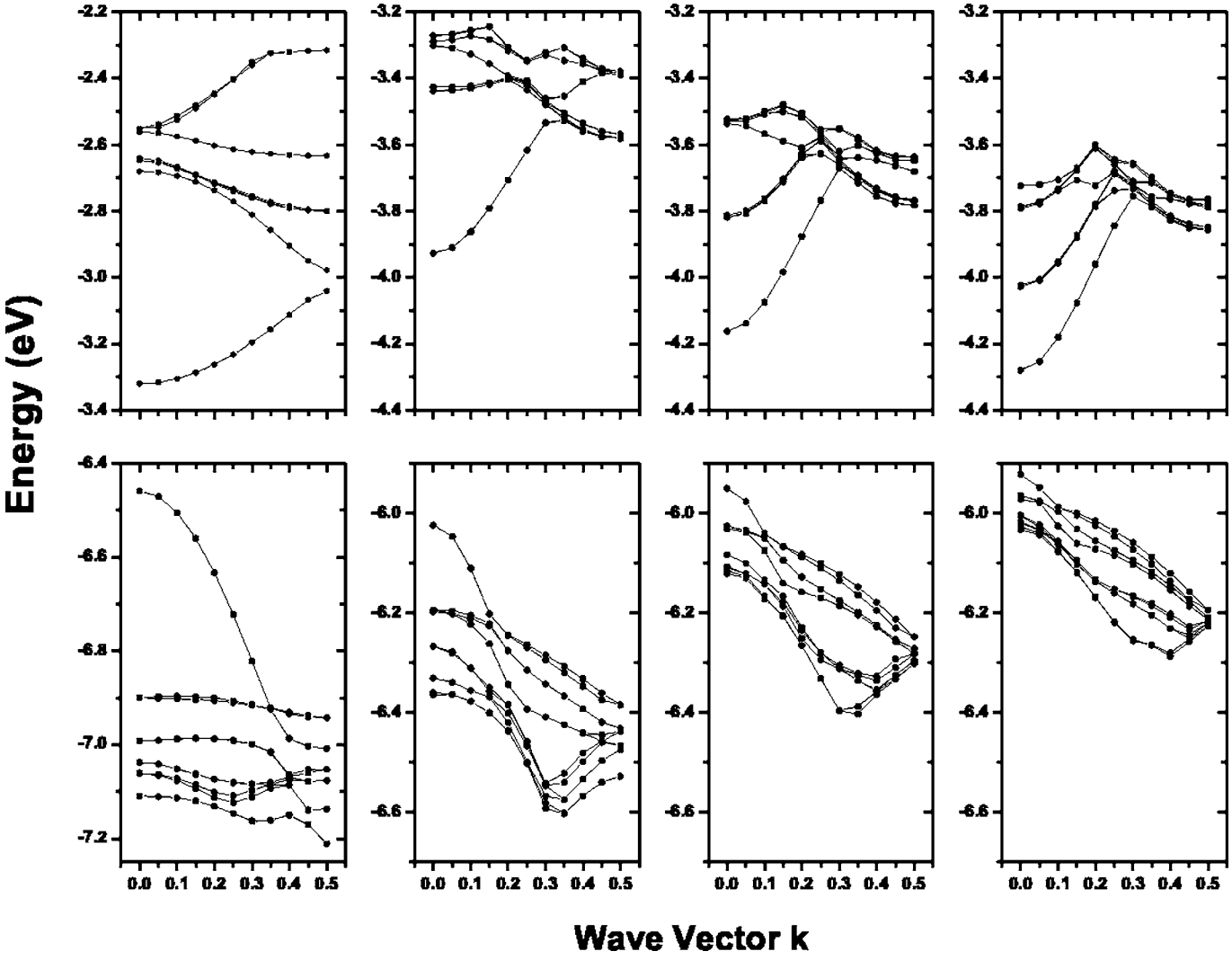

FIG. 3. Same as in Fig. 1, but for the [111] wires of different sizes. The wave vector is in units of $\frac{2\pi}{\sqrt{3}a}$.

ent crystallographic axes, our calculations show another interesting conclusion, that is, the [111] wires offer both stronger optical intensity *and* higher polarization ratio for a given wire diameter, which we hope to be a useful guide when one engineers the crystallographic axis of nanowires for better performance.

Our theoretical results thus confirm the orbital-induced origin,[13–18] rather than the dielectric confinement, for the highly polarized photoluminescence that was observed in semiconductor nanowires.[7] While our pseudopotential calculations do consider the existence of vacuum environment, this inclusion is however not related with the dielectric confinement. Note that the magnitude of electric field of the excitation power and the dipole matrix are two independent quantities in determining the absorption intensity[24] (also polarization ratio). The dielectric confinement manifests itself by affecting the electric field that penetrates into the wire, while the dipole matrix is determined by the electron wave functions. The strong polarization ratio, shown in Fig. 5, is computed using the dipole matrices and thus results from the specification of electronic states that are intrinsic to nanowires. The theoretical polarization ratio of more than 90%, as found in our calculations, is comparable with the experimental value of 95%.[7]

In real experiments, it is likely that intrinsic electron properties and dielectric confinement both contribute to the observed high polarity of photoluminescence. Identifying certain observable characteristic difference to further distinguish these two mechanisms may thus be useful. We would like to point out that such a difference indeed exists, that is, the size dependence of the polarization ratio. As the wire diameter shrinks, the dielectric contrast between the wire and its environment decreases, since the confinement leads to an enlarged band gap and thus a smaller dielectric constant for the wire. As a result, the polarization ratio arising from the dielectric confinement is to *decrease* when wire becomes smaller. On the other hand, and as revealed by our calculation results in Fig. 5, the polarization ratio arising from the intrinsic electronic states is to *increase* as the size becomes smaller. Experimental measurements on the size dependence of polarization ratio in nanowires may thus help to show more insight on these two mechanisms.

It should be pointed out that our transition rate and polarization ratio are calculated without considering the electron-

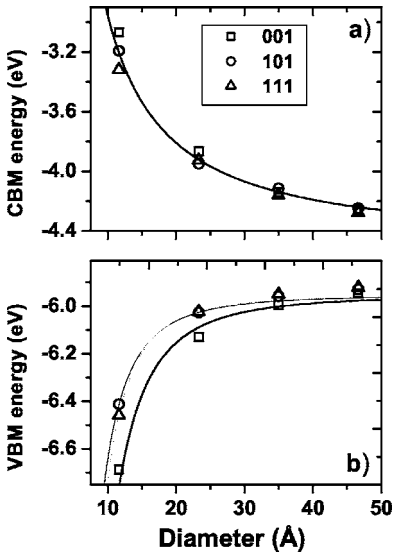

FIG. 4. Energies of (a) the CBM and (b) the VBM at the zone center as a function of wire diameter, for the [001] wires (squares), the [101] wires (circles), and the [111] wires (triangles). Symbols are from direct calculations; lines are analytical fitting results. For CBM, only the fitting curve for the [101] wires is given for the sake of clarity.

hole Coulomb interaction. This approach is likely valid for strong confinement region since electron states are well separated in energy. Although the electron-hole binding also increases as the confinement becomes stronger, this increase is much smaller as compared to the increase in the single-particle energy separation. As a consequence, the Coulomb interaction (as a perturbation) does not mix significantly the single-particle wave functions in the strong confinement region. Computing the transition rate by use of single-particle wave functions is thus a reasonable approximation. We expect the effect of the wave function mixing due to the electron-hole interaction to become increasingly important as the wire size is large, where more sophisticated approach such as solving the Bethe-Salpeter equation is needed.[38]

Electron and hole effective masses. One of critical quantities that determine carrier mobility is effective mass. While carrier mobility in bulk semiconductors is rather well measured, the mobility in nanowires remains interesting to be investigated both experimentally and theoretically. Here we

TABLE I. The A and α parameters resulting from the analytic fitting of the single-particle energies of our direct pseudopotential calculations. The A and α values for spherical InP dots are also given for comparison.

Systems	CBM	CBM	VBM	VBM
	A	α	A	α
001 wires	35.03	1.2924	−454.21	2.5802
101 wires	22.66	1.1671	−325.38	2.6743
111 wires	23.58	1.2040	−586.43	2.8748
dots	15.10	0.9296	−119.08	1.8443

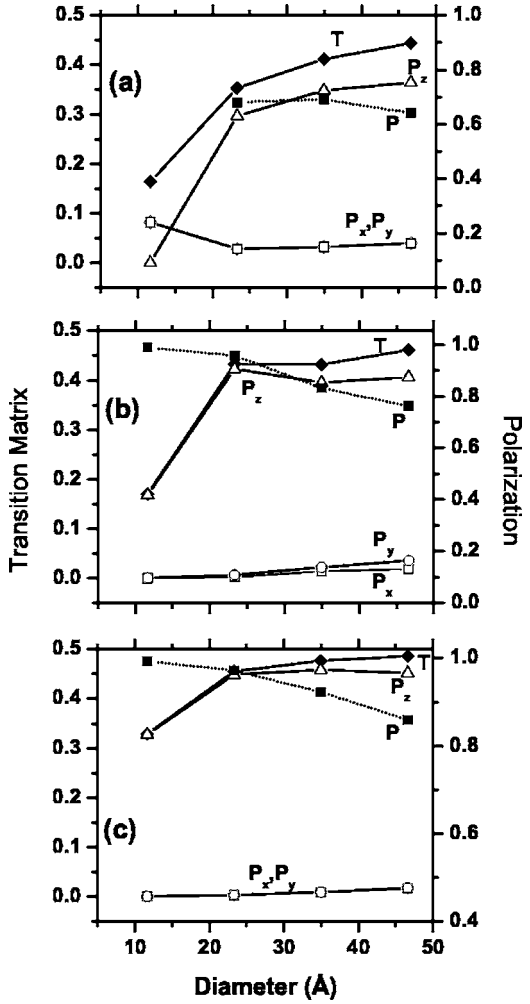

FIG. 5. Transition matrix T, individual components P_i ($i=x,y,z$), and polarization ratio P for InP wires of different crystallographic axes: (a) the [001] wires, (b) the [101] wires, (c) the [111] wires. T is shown as filled diamonds and solid line, and polarization ratio as filled squares and dotted line. All quantities are described using the left vertical axis (of which the scale is in units of $1/\text{Bohr}^2$), except the polarization ratio which is described using the right vertical axis.

study how the effective mass may vary in nanowires of different orientations and different sizes. It has been known that one needs to be cautious in determining effective mass when spin-orbit (SO) coupling is included in the calculation. We have performed two types of calculations: one with SO included, but with the average orbital energy over SO-split states used to determine the effective mass; another with SO coupling turned off. Two types of calculations yield similar effective masses. Here we show in Fig. 6 the results obtained from the calculations without spin-orbit coupling, for electron and for hole at the zone center. For electron [Fig. 6(a)], the mass is found to increase with the decreased diameter, demonstrating that the effective mass is size dependent. Note that, while optical band gap in nanostructures has been amply shown to depend considerably on size, the size dependency of the effective mass is however less known and understood. This dependence suggests that one needs to be

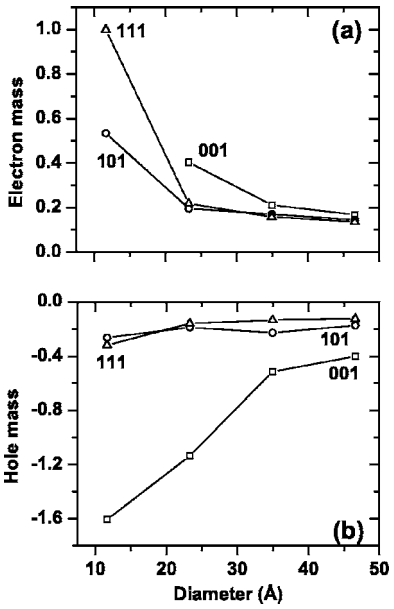

FIG. 6. (a) Electron and (b) hole effective masses as a function of wire diameter for InP wires of different crystallographic axes. For the $D=11.7$ Å wire along the [001] direction, the electron mass is calculated to be ~10 in magnitude because of the occurrence of an indirect band gap, and is not shown in the figure.

cautious when assuming effective mass to be constant in theoretical calculations of semiconductor nanostructures. Our results [Fig. 6(a)] also show that, for a given size, the [001] wires have slightly larger electron mass as compared to wires along two other directions.

The perhaps most striking results on carrier masses in semiconductor wires concern the hole masses as shown in Fig. 6(b). First, the three types of wires show a drastic difference in the manner of how their hole masses depend on the wire diameter. For the [001] wires, the calculated hole mass displays a significant dependence on the size, varying by a factor of 4 from $m_h^*=1.6$ in the $D=11.7$ Å wire to $m_h^*=0.4$ in the largest wire considered. On the other hand, the hole masses of the [101] and [111] wires are found to be nearly a constant, which persists down to a very small diameter of 11.7 Å. This predicted size insensitivity of the hole effective mass is particularly attractive in terms of obtaining high carrier mobility in nanowire circuits when the size of wire becomes smaller.

Second, our realistic calculations determine the hole masses in the [101] and [111] wires to be ~0.2, which are remarkably smaller than the hole effective mass in *bulk* InP. More specifically, the hole mass in bulk is calculated to be 2.45 along the [101] direction and 1.03 along the [111] direction, obtained from the same screened pseudopotential as used in wire calculations. Our results thus demonstrate an important conclusion, namely, that the carrier masses in semiconductor wires can be drastically reduced—and consequently, the carrier mobility can be significantly enhanced—when going from bulk to nanowires. To illustrate more quantitatively how the reduction of the hole mass m_h^* in nanowires may affect the carrier transport, we estimate the mobility μ_h by recognizing that μ_h in semiconductor is proportional[39] to $|m_h^*|^{-5/2}$. The ten fold decrease in m_h^*, when going from bulk to the [101] wires, is able to increase the mobility by five hundred times as holes move along the same [101] direction in both cases. Our study thus implies that engineering crystallographic orientation is indeed an efficient route that is able to provide new material properties in semiconductor nanowires.

The interstate coupling among bulk electron states, which occurs when forming the wire states, is found to be responsible for the small effective mass in the [101] and [111] wires. To explain this, we begin by expanding the *wire* wave function $\Psi_{\mathbf{q}}^{\text{wire}}$ of wave vector $\mathbf{q}$ as a linear combination of *bulk* wave functions $\chi_{n\mathbf{k}}^{\text{bulk}}$ of band n and wave vector $\mathbf{k}$, i.e.,

$$\Psi_{\mathbf{q}}^{\text{wire}} = \sum_{n\mathbf{k}} C_{n\mathbf{k}} \chi_{n\mathbf{k}}^{\text{bulk}}, \tag{1}$$

where $C_{n\mathbf{k}}$ is the expansion coefficient.[37] Neglecting the surface effects (which was shown to be a good approximation for bulk like states in nanostructures[37]), one can obtain the relationship of orbital energies in nanowire and in bulk as $E_{\mathbf{q}}^{\text{wire}}=\Sigma_{n\mathbf{k}}|C_{n\mathbf{k}}|^2 E_{n\mathbf{k}}^{\text{bulk}}$. Considering that the coefficients $C_{n\mathbf{k}}$ do not vary, to the first-order perturbation, for two close $\mathbf{q}$'s that are used to determine the effective mass of wire (but the bulk $\mathbf{k}$ points that contribute in forming the wire states are changing with $\mathbf{q}$ accordingly), one can determine the effective mass in wire to be $(1/m^*)_{\text{wire}}=\Sigma_{n\mathbf{k}}\frac{1}{\hbar^2}|C_{n\mathbf{k}}|^2\nabla_{\mathbf{k}}^2 E_{n\mathbf{k}}^{\text{bulk}}$. In other words, the effective mass of wire depends on the curvature of the *bulk* dispersion at those $\mathbf{k}$ points that contribute when forming the wire state. Since determining $C_{n\mathbf{k}}$ is time consuming, we only consider the [001] wire and the [111] wire of $D=35.0$ Å as an example. For the [001] wire, this approach yields a hole mass of 0.50, close to the direct calculation result of 0.52 in Fig. 6(b). For the $D=35.0$ Å [111] wire, the above approach predicts a hole mass of 0.22, as compared to the value of 0.13 in our direct calculation, and is found to be indeed much smaller than the bulk effective mass (1.03) along the [111] direction.

Equation (1) can be further used to explain why the magnitude of transition matrix element declines as the wire becomes smaller (as observed in Fig. 5). For this, let us first point out the following two facts. (i) In the right side of Eq. (1) there is a dominant contribution from some specific bulk $\mathbf{k}$ points, as demonstrated previously.[40] In fact, if we denote those $\mathbf{k}$ points of dominant contribution as $\mathbf{k}_0$, then the magnitude of $\mathbf{k}_0$ is related with the D diameter of wire by[41] $|\mathbf{k}_0|\sim\frac{1}{D}$. The transition matrix element in *wire* can thus be approximated described by the VBM-to-CBM transition matrix element at $\mathbf{k}_0$ in *bulk*. (ii) We numerically found that, for *bulk* Bloch states, the magnitude of the transition matrix element between the highest valence state and the lowest conduction state is at its maximum at the zone center, and declines as wave vector $\mathbf{k}_0$ moves away from Γ. When the wire diameter decreases, the *bulk* $\mathbf{k}_0$ points in Eq. (1) that contribute predominantly in forming the band-edge states of the wire shift away from the center of the bulk Brillouin zone. This causes the transition matrix element in wire (which can be approximately described by the counterpart at $\mathbf{k}_0$ in bulk) to decline, which is consistent with the result in Fig. 5.

The unusual hole effective masses in the [101] and [111] wires give rise to another interesting question, that is, how effective masses in these wires approach the bulk values as the wire diameter continues to increase. In fact, it seems in Fig. 6(b) that the m_h^* hole masses from direct calculations, for the considered size range in our study, do not appear to approach their bulk counterparts. This is puzzling. We now show that possible existence of an electronic phase transition, which occurs for wires of larger diameter, provides an answer to this question. Let us look at the [111] wires. By examining the *valence* band structure of the $D=11.7$ Å wire in Fig. 3, we find that the first band and the second (or the third) band have very different dispersions: the former is steep with a small hole mass while the latter is flat with a large mass. These two bands cross at $\mathbf{k}\approx 0.35\frac{2\pi}{\sqrt{3}a}$ for the $D=11.7$ Å wire. As the diameter of wire increases, the energy separation between the first and second bands is significantly reduced as a result of their different size dependence. Meanwhile, the crossing point between these two bands moves closely to Γ (e.g., to $\mathbf{k}\approx 0.1\frac{2\pi}{\sqrt{3}a}$ in the $D=46.6$ Å wire). As the size further increases, the second band is expected to continue its upshift faster than the first band, and eventually becomes the top valence band with its effective mass approaching the bulk value. Though our computing facility does not allow us to perform direct calculations for very large wires, our results of the smaller wires clearly show a possible trend for the occurrence of the above transition. In difference with the heavy hole/light hole level exchange in quantum wells which is mainly caused by lattice mismatch between well and barrier materials,[19,22,23] the level exchange, as revealed here in free-standing nanowires without strain, results from size effects which produce different confinement shifts for different bands.

IV. CONCLUSIONS

We have performed rather systematic pseudopotential calculations on InP nanoscale quantum wires with different crystallographic axis and with different size. We have studied the band dispersion, scaling law of orbital energies, size dependence of transition intensity, optical polarization ratio, and electron/hole effective masses, as well as the influence of crystallographic axis on these properties. The specific findings that we have obtained from these studies are summarized as follows.

(i) The lowest conduction bands of the [001] and [111] wires, but not the [101] wires, are revealed to possess a hump in their dispersions. These humps could be confirmed by inverse photoemission measurements. Our results further show the formation of clearly observable subbands in the conduction states when the diameter of wire ranges from 30 –50 Å. (ii) For all three types of wires studied, the lowest *conduction* states at zone-boundary X point are found to have an appreciable size confinement effect. Meanwhile, the orbital energy of the top *valence* state at the X point is predicted to depend significantly on the crystallographic axis. More specifically, for the same diameter $D=46.6$ Å, the VBM at X is found to locate near −6.8 eV in the [001] wire, but near −6.2 eV in the [101] and [111] wires. As a result, the bandwidth of the highest valence band differs significantly in differently oriented wires. (iii) The scaling α exponent is found to be nearly universal, independent of the wire orientation, despite the fact that the A coefficient and thus the confinement energy vary with crystallographic axis. Quantitatively, α is determined to be $\sim$2.7 for the VBM and $\sim$1.2 for the CBM at the zone center Γ. Furthermore, the α exponent in InP wires is shown to be substantially different from that in InP dots. In other words, our study explicitly demonstrates that α is dimensionality dependent. (iv) We find that the magnitude of the transition matrix element decreases as the wire diameter becomes smaller. However, and interestingly, polarization ratio in nanowires is found to behave in a drastically different fashion—it *increases* with the decreasing size. (v) As size becomes smaller, the magnitude of transition matrix deteriorates most for the [001] wires, and least for the [111] wires. The [111] wires are thus more suitable for optical applications when small size is needed. (vi) A large polarization ratio of $\sim$90% is found to exist in the [101] wires and in the [111] wires, depending on the wire diameter. This finding provides another possible mechanism, other than the dielectric confinement model, to explain the highly polarized photoluminescence observed in experiments. (vii) In contrast with what is commonly assumed in the literature, the electron effective mass is found to depend significantly on the wire diameter. (viii) For the [001] wires, the calculated hole mass is found to be widely tunable from 1.6 to 0.4 by varying the wire size. However, the hole masses in the [101] and [111] wires are found to depend little on the size. (ix) Our calculations demonstrate that, for a given carrier mobility direction, it is possible for the hole mass to be much smaller than that in bulk, and consequently, it is likely to obtain in nanowires much higher mobility that is not available in bulk. This unusual small hole mass is found to result from an interesting electronic band transition that occurs in nanowires.

ACKNOWLEDGMENTS

We thank A. Nazzal for useful discussions. This work was partially supported by the Oklahoma-Arkansas MRSEC.

[1] Y. Huang, X. Duan, Y. Cui, L. J. Lauhon, K.-H. Kim, and C. M. Lieber, Science **294**, 1313 (2001).

[2] N. I. Kovtyukhova and T. E. Mallouk, Chemistry (Weinheim, Ger.) **8**, 4354 (2002).

[3] R. S. Friedman, M. C. McAlpine, D. S. Ricketts, D. Ham, and C. M. Lieber, Nature (London) **434**, 1085 (2005).

[4] A. Kraft, Chem. Ind. **11**, 30 (2005).

[5] M. H. Huang, S. Mao, H. Feick, H. Yan, Y. Wu, H. Kind, E.

Weber, R. Russo, and P. Yang, Science **292**, 1897 (2001).
[6] X. Duan, Y. Huang, R. Agarwal, and C. M. Lieber, Nature (London) **421**, 241 (2003).
[7] J. Wang, M. S. Gudiksen, X. Duan, Y. Cui, and C. M. Lieber, Science **293**, 1455 (2001).
[8] F. Buda, J. Kohanoff, and M. Parrinello, Phys. Rev. Lett. **69**, 1272 (1992).
[9] X. Zhao, C. M. Wei, L. Yang, and M. Y. Chou, Phys. Rev. Lett. **92**, 236805 (2004).
[10] J. Li and L.-W. Wang, Phys. Rev. B **72**, 125325 (2005).
[11] T. M. Schmidt, R. H. Miwa, P. Venezuela, and A. Fazzio, Phys. Rev. B **72**, 193404 (2005).
[12] C. E. Pryor and M.-E. Pistol, Phys. Rev. B **72**, 205311 (2005).
[13] P. C. Sercel and K. J. Vahala, Appl. Phys. Lett. **57**, 545 (1990).
[14] U. Bockelmann and G. Bastard, Phys. Rev. B **45**, 1688 (1992).
[15] G. Goldoni, F. Rossi, E. Molinari, A. Fasolino, R. Rinaldi, and R. Cingolani, Appl. Phys. Lett. **69**, 2965 (1996).
[16] P. C. Sercel and K. J. Vahala, Phys. Rev. B **44**, 5681 (1991).
[17] M. P. Persson and H. Q. Xu, Phys. Rev. B **70**, 161310(R) (2004).
[18] A. V. Maslov and C. Z. Ning, Phys. Rev. B **72**, 161310(R) (2005).
[19] D. S. Citrin and Y. C. Chang, Phys. Rev. B **40**, 5507 (1989).
[20] J. Hu, L.-S. Li, W. Yang, L. Manna, L.-W. Wang, and A. P. Alivisatos, Science **292**, 2060 (2001).
[21] X. Chen, A. Nazzal, D. Goorskey, M. Xiao, Z. Adam, and X. Peng, Phys. Rev. B **64**, 245304 (2001).
[22] T. A. Ma and M. S. Wartak, Phys. Rev. B **50**, 15401 (1994).
[23] R. W. Martin, S. L. Wong, R. J. Warburton, R. J. Nicholas, A. D. Smith, M. A. Gibbon, and E. J. Thrush, Phys. Rev. B **50**, 7660 (1994).
[24] P. Yu and M. Cardona, *Fundamentals of Semiconductors* (Springer, Berlin, 2001).
[25] W. Kohn and L. J. Sham, Phys. Rev. **140**, A1133 (1965).
[26] M. S. Hybertsen and S. G. Louie, Phys. Rev. B **34**, 5390 (1986).
[27] W. Su, X. Huang, J. Li, and H. Fu, J. Am. Chem. Soc. **124**, 12944 (2002).
[28] N. A. Hill and K. B. Whaley, Phys. Rev. Lett. **75**, 1130 (1995).
[29] G. W. Bryant and W. Jaskolski, Phys. Rev. B **67**, 205320 (2003).
[30] G. Allan and C. Delerue, Phys. Rev. B **70**, 245321 (2004).
[31] A. Franceschetti and A. Zunger, Phys. Rev. Lett. **78**, 915 (1997).
[32] L. W. Wang and A. Zunger, Phys. Rev. B **59**, 15806 (1999).
[33] P. C. Sercel and K. J. Vahala, Phys. Rev. B **42**, 3690 (1990).
[34] H. Fu and A. Zunger, Phys. Rev. B **55**, 1642 (1997); L. W. Wang and A. Zunger, *ibid.* **51**, 17398 (1995).
[35] G. B. Bachelet, D. R. Hamann, and M. Schluter, Phys. Rev. B **26**, 4199 (1982).
[36] L. W. Wang and A. Zunger, J. Chem. Phys. **100**, 2394 (1994).
[37] H. Fu, Phys. Rev. B **65**, 045320 (2002).
[38] M. Rohlfing and S. G. Louie, Phys. Rev. Lett. **81**, 2312 (1998).
[39] J. M. Ziman, *Electron and Phonons* (Oxford University press, London, 1963).
[40] H. Fu, L. W. Wang, and A. Zunger, Phys. Rev. B **57**, 9971 (1998).
[41] M. V. Rama Krishna and R. A. Friesner, Phys. Rev. Lett. **67**, 629 (1991).